CFD VALIDATION STUDY OF NEXST-1 NEAR MACH 1

Keizo Takenaka*, Kazuomi Yamamoto, Ryoji Takaki****

**Mitsubishi Heavy Industries, Ltd., 10 Oye-cho, Minato-ku, Nagoya, 455-8515,*

***Japan Aerospace Exploration Agency Institute of Space Technology and Aeronautics, 7-44-1 Jindaiji-higashi, Mitaka, 182-8522, Japan*

Keywords: *CFD, validation, NEXST-1, Mach1, Wall interference*

Abstract

Development of a next generation airplane, which cruises near sonic speed, received considerable attention in 2002. To investigate aerodynamic characteristics and validity of CFD codes as a design tool in this new cruise condition, detailed wind tunnel test and CFD validation study was conducted in near sonic regime about the NEXST-1, unpowered supersonic experimental vehicle as a cooperative research program between JAXA (Japan Aerospace Exploratory Agency) and MHI (Misubishti-Heavy Industries, Ltd.). The intensive CFD study showed satisfactory agreement with WTT results in general, even near sonic speed. It was found an airplane with very thin airfoil tended to have a drag dip at moderate (cruise) lift condition in high transonic region due to its less wave drag increase. It was also found the dip was overpredicted in the wind tunnel test due to the buoyancy effects induced by wind tunnel wall and sting for model support.

1 Detailed Transonic Wind Tunnel Test

As the first step, we conducted a detailed transonic wind tunnel test of the 8.5% force model of the NEXST-1 (unpowered National Experimental Supersonic Transport[1]) at 2m×2m continuous transonic wind tunnel of JAXA[2] to obtain basic aerodynamic characteristics of the NEXST-1 configuration, which was to be used in the CFD validation study. Fig.1 shows the WTT model installed in the test section with 6% porosity slotted–walls. The span of the model was 401mm and Reynolds number based on MAC was approximately 2.5million. Measurement items were six-component force and moment by internal balance, and surface pressure distributions by PSP (Pressure Sensitive Paint). Measurements were focused on near sonic regime, which was Mach 0.90 to 1.05.

2 CFD validation study

2.1 Computational method

Following WTT, both MHI and JAXA conducted CFD analysis. MHI used in-house single/overset structured mesh code called JANET, and JAXA used in-house multi-block structured mesh code called UPACS[3][4].

Table 1 shows specifications of computational mesh and computational method and Fig.2 shows computational mesh of MHI. Configuration of CFD is WTT model with the sting and CFD simulates the identical transition location with the WTT model trip disk location (3% chord of the wing).

2.2 Computational results

Fig.3 shows the typical flow characteristics about NEXST-1 in high transonic speed, which are streamlines around the vortex core and separated region at Mach number 0.98, angle of attack from 0 to 4deg. In the figure, red line shows separated region. Though there is no vortex around the wing at angle of attack 0deg, as angle of attack increases, vortex is generated around the leading edge of the wing. Due to the

vortex, separation occurs around the outboard wing station.

Fig.4, Fig.5 and Fig.6 show the comparison of aerodynamic forces with WTT results at Mach number 0.95. In Fig.6, Error bar shows the drag repeatability of WTT, which are roughly 10 counts. Lift and pitching moment agree well. But, drag of WTT showed interesting characteristics. The drag polar of the WTT was different from that measured in another WTT using the same model and porous cart (20% of porosity). Predicted drag of CFD showed excellent agreement with WTT using porous wall cart within accuracy of measurements. There arises concern about wall-interference. Another interesting characteristics were observed in the drag divergence characteristics. The drag of WTT near sonic regime dropped as much as 20-30cts. at any lift condition. CFD also predicted the above-mentioned drag-dip phenomenon at moderate lift condition and this phenomenon was also observed in the flight model CFD analysis (Fig.7). However, at low lift condition CFD didn't predict the drag-dip (Fig.8). What is more, at such condition, friction drag is dominant with total amount of the drag in CFD results and the amount of pressure drag is not enough accounting for the drag-dip. We investigated the mechanism of the drag-dip phenomenon. Results of the investigation are described in the next section.

2.3 Mechanism of the drag-dip phenomenon

From the drag divergence characteristics of CFD results at moderate lift condition, we found the drag-dip was due to pressure drag decrease in the outboard wing, though the span wise lift distributions didn't change much (Fig.9, Fig.10). In Fig.10, C* is the local chord length normalized by MAC. What is more, from the close look of section pressure distributions, we found the drag dip occurred because induced drag reduction due to angle of attack decrease was superior to wave drag increase at the same lift condition (Fig.11, Fig.12). In general, wave drag increase is dominant when Mach number increases, but we found thin airfoil such as NEXST-1 (roughly 3% thickness) has the possibility of such phenomenon by the 2D airfoil analysis (Fig.13). Airfoils we used are typical supercritical airfoil and their thicknesses are 2.5,5.0 and 7.5% each. 2.5% and 5.0% thickness airfoils were made simply by modifying 7.0% thickness airfoil. The 2.5% thickness airfoil has the drag-dip characteristics. And what is more interesting, even in the airfoil, at low lift condition, the drag-dip was not observed and the amount of pressure drag is not enough accounting for the drag-dip (Fig.14). At that condition, another reason should be investigated.

3 Further investigations for assessment and improvement of CFD and WTT

3.1 Results of the investigations

As just described, CFD showed satisfactory agreement with WTT overall, however, there were still some discrepancies between CFD & WTT such as drag-dip. Therefore, several analyses on factors, which could cause the difference between CFD and WTT, were conducted as the next step. Table2 shows major investigated items.

Grid dependency and far-field treatment through the validation study was found no problem. Also, we adopt fixed transition analysis and this was proved the better choice in terms of prediction of the leading edge vortex formation (Fig.15, Fig.16). Aeroelastics effect of the WTT model was found negligible by static aeroelastic analysis.

Finally, through these investigations, we found the sting and tunnel wall had significant impacts on drag estimation in such high transonic regime.

3.2 Wall and sting effects

In Fig.7, though CFD of Flight model and WTT model showed the same drag divergence characteristics, drag level is different and the drag divergence Mach number is also different by 0.01. From comparison of pressure distribution, we found the sting causes large adverse pressure gradient (buoyancy effect) on the model (Fig.17). This effect was effectively observed around V-tail (Fig.18). Fig. 19 shows a comparison of pressure distribution between Flight model and WTT model. Due to the buoyancy effect, pressure distribution of the WTT model shifts positive side. Fig.20 shows the increment drag between these two models. Every component was affected and the total difference of the drag was roughly 10cts.

Because such huge effect of buoyancy and the difference of the drag divergence characteristics between CFD and WTT associated with the concern of the wall effects, we decided to conduct the complete wind tunnel simulation using UPACS. Fig.21 shows the computational grid of JAXA 2m×2m transonic wind tunnel. Total grid points are approximately 10million. Grid includes tunnel wall, slot, plenum chamber and plenum exhaust. Wall & slot are treated as inviscid. Fig.22 shows Mach number distribution at slot located plane. Flow of the test section blew out to the plenum. Fig.23 shows comparison of pressure contours between free-air (WTT model) and wind-tunnel analysis at angle of attack 0 deg. Obviously, as Mach number increases, buoyancy induced by wall-sting interaction becomes strong. Fig.24 shows the drag divergence characteristics. CFD of slotted wall configuration shows the drag-dip compared with free-air with sting configuration, though not quantitatively agree.

4 Concluding remarks

Through detailed transonic wind tunnel test near sonic speed and CFD validation study, following conclusions are drawn.

- CFD showed satisfactory agreement with WTT overall, even near sonic speed.
- We found thin-airfoil such as NEXST-1 tended to have the drag-dip characteristics due to less wave drag increase.
- Through several investigations, our CFD was assessed and found the reason of discrepancy between CFD and WTT lay in buoyancy effects induced by wall and sting.
- We found buoyancy effect induced by wall-sting interference caused the drag-dip at low lift condition in this test.
- Appropriate buoyancy correction method or testing technique that decreases buoyancy effect, should be developed in such high transonic regime.

Acknowledgement

The authors would like to express special thanks to Dr. Kenji Sakai of JAXA, and Mr. Yuichi Shimbo of Mitsubishi Heavy Industries, Ltd. for their sincere cooperation to the present work.

References

[1] Yoshida K., Overview of NAL's Program Including the Aerodynamic Design of the Scaled Supersonic Experimental Airplane, RTO-EN-4, Nov. 1998

[2] National Aeronautical Laboratory, "Design and Construction of the 2m×2m Transonic Wind Tunnel at the National Aeronautical Laboratory", TECHNICAL REPORT OF NATIONAL AERONAUTICAL LABORATORY TR-25, 1962 (in Japanese)

[3] Yamane, T., Yamamoto, K., Enomoto, S., Yamazaki, H., Takaki, R., and Iwamiya, T., "Development of a Common CFD Platform - UPACS -," in Parallel Computational Fluid Dynamics - Proceedings of the Parallel CFD 2000 Conference, Trondheim, Norway, Elsevier Science B. V., 2001, 257-264.

[4] Takaki, R., Yamamoto, K., Yamane, T., Enomoto, S., and Mukai, J., "The Development of the UPACS CFD Environment," in High Performance Computing – Proceedings of 5th International Symposium, ISHPC 2003, Ed. Veidenbaum *et. al.*, Springer, 2003, pp307-319.

Table 1 Specification of computational mesh and computational method

		JAXA UPACS	MHI JANET
Grid	Mesh system	Multi-Block structured mesh (88blocks)	Stuructured mesh
	Total grid points	6 million	2.4 million
Flow Solver	Governing equation	Thin layer Reynolds-averaged Navier-Stokes	
	Time integration	Matrix-free Gauss Seidel	LU-ADI
	Convection term	Roe + MUSCL	Roe + MUSCL
	Turbulence model	Spalart-Allmaras	Baldwin-Lomax

Table 2 Investigated items for assessment & improve of CFD & WTT

Purpose	Investigated Items	Overview of the analysis	Results
Assessment of CFD	Grid dependency	Grid convergence study	Negligible
	Far-field treatment	Far-field size, Far-field boundary condition treatment	Negligible
	Transition effect	Fully turbulent & Forced transition	Forced transition is the better
Investigation and Improvement of CFD & WTT	Aeroelastics	Static aeroelastic analysis	Negligible
	Sting effects	W/WO Sting	Significant
	Wall effects	W/WO WT wall	Significant

Fig.1 NEXST-1 8.5% WTT model

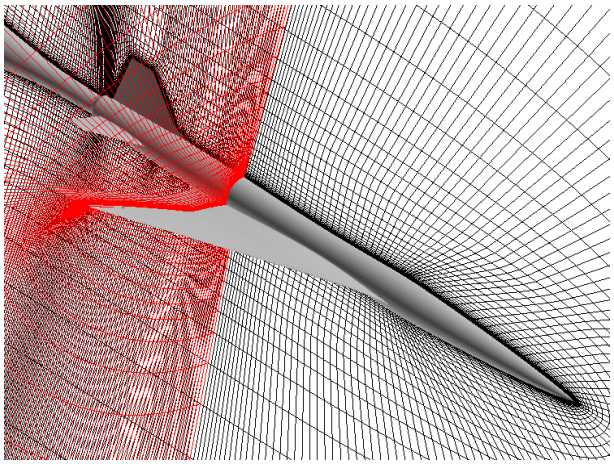

Fig. 2 Computational mesh of MHI

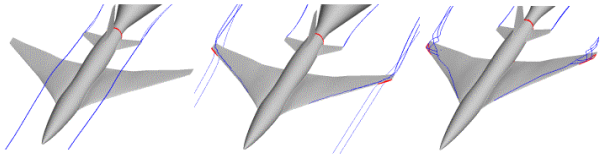

Fig. 3 Streamlines around vortex core at M=0.98 (left: α=0°, mid: α=2° right: α=4°)

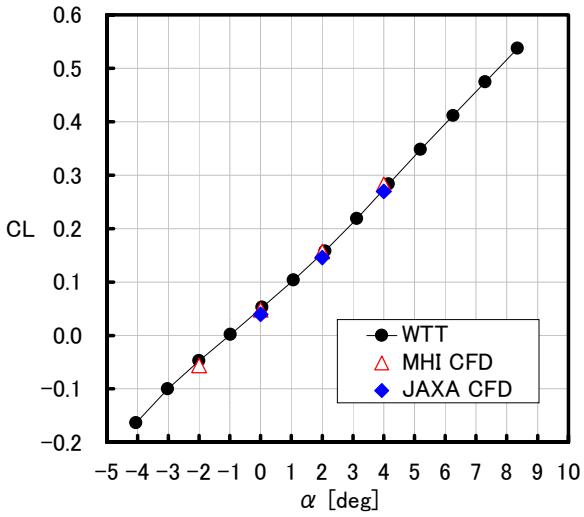

Fig. 4 CL-α at M=0.95

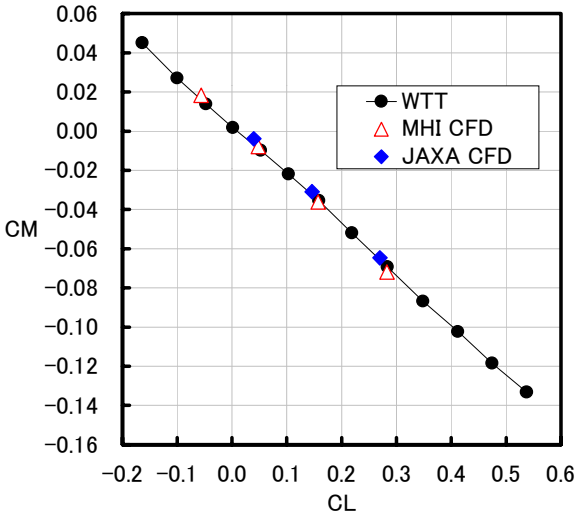

Fig. 5 CM-CL at M=0.95

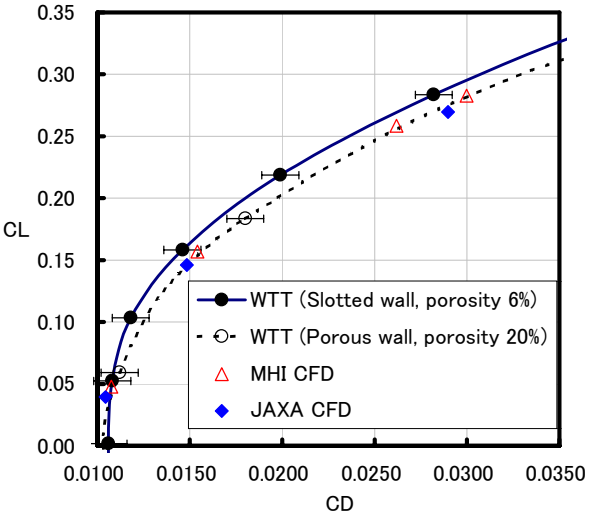

Fig.6 Drag polar characteristics at M=0.95

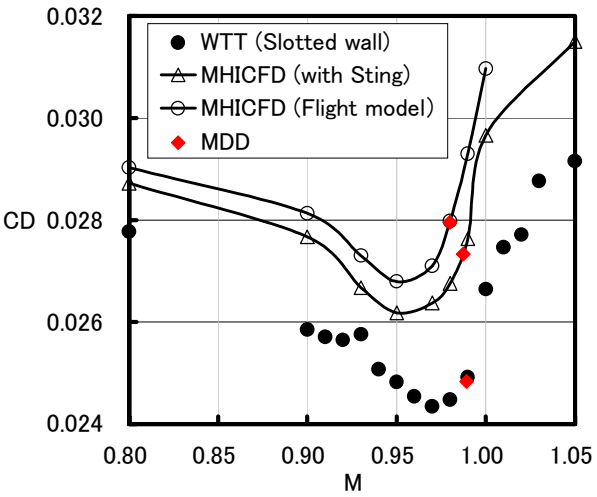

Fig.7 Drag divergence characteristics at CL=0.26

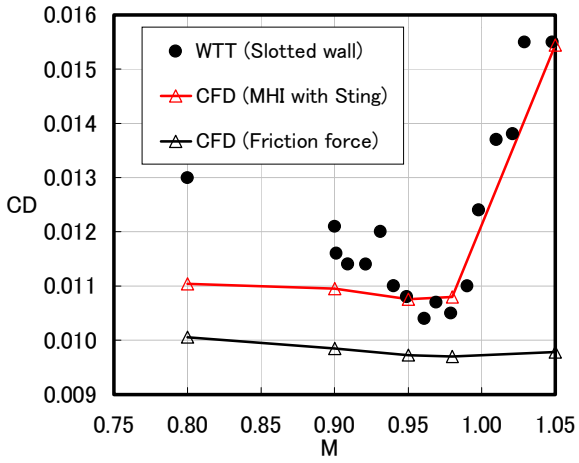

Fig.8 Drag divergence characteristics at α=0 °

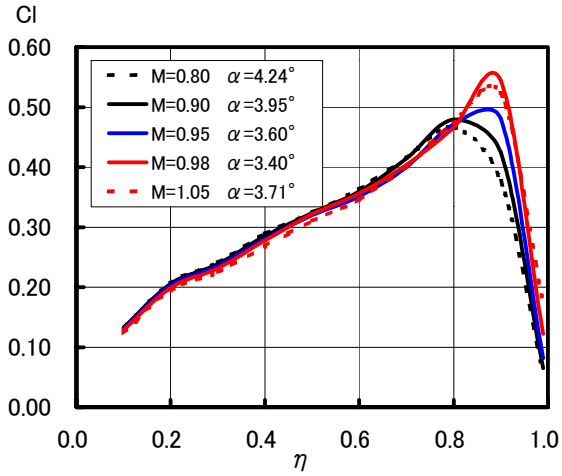

Fig.9 Span wise lift distributions at CL=0.26

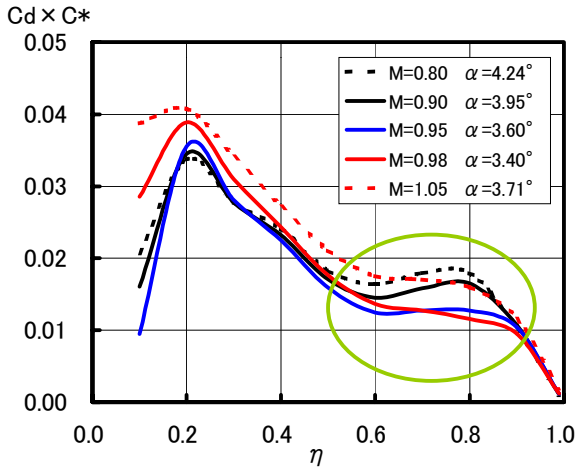

Fig.10 Span wise pressure drag distributions at CL=0.26

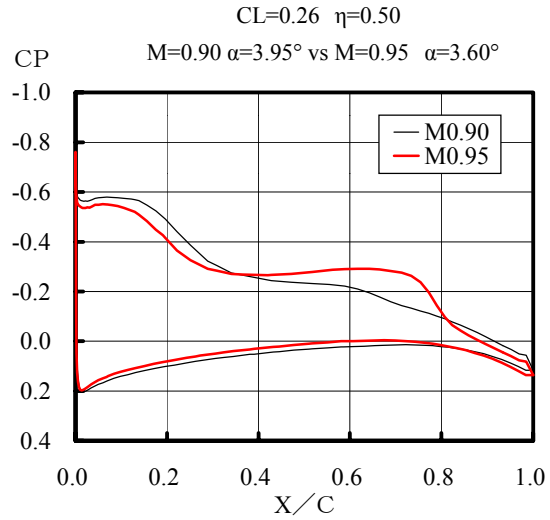

Fig.11 Comparison of pressure distributions at 50%span

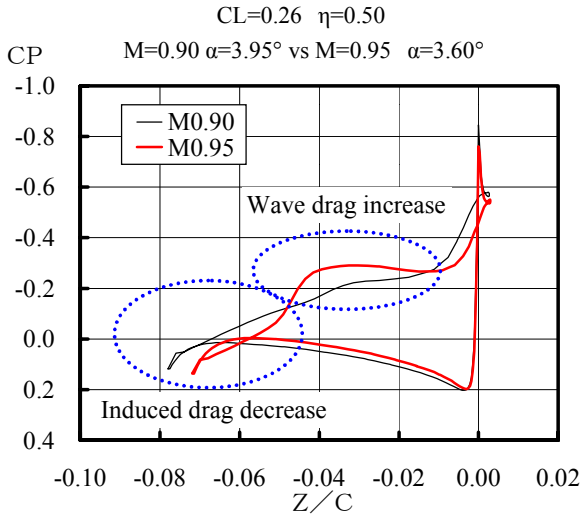

Fig.12 Comparison of drag loop at 50%span

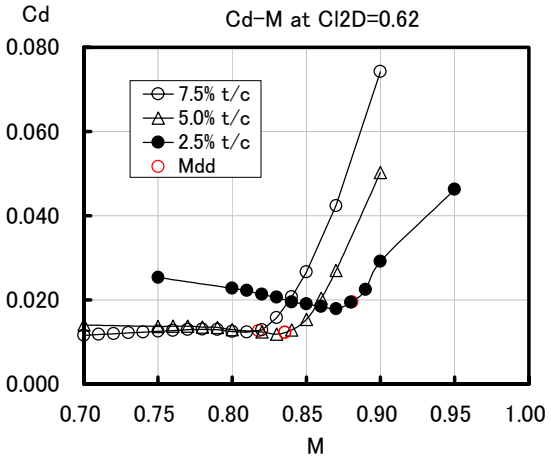

Fig.13 Drag divergence characteristics of 2D airfoil at Cl=0.62

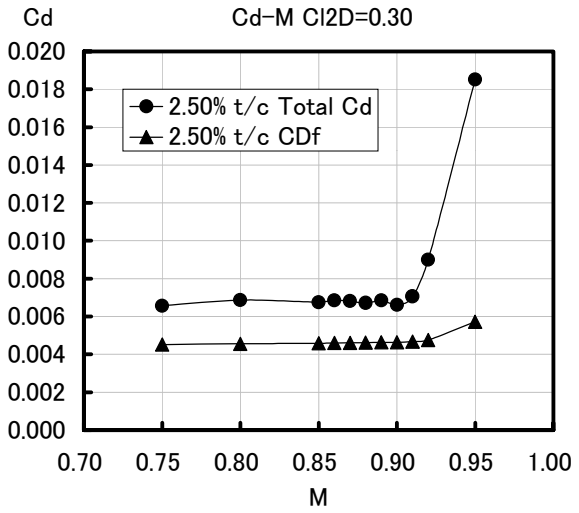

Fig.14 Drag divergence characteristics of 2D airfoil at Cl=0.30

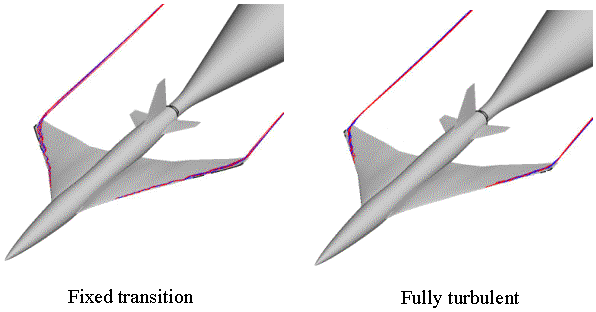

Fig.15 Streamlines around the vortex core at M=0.95, α =2 °

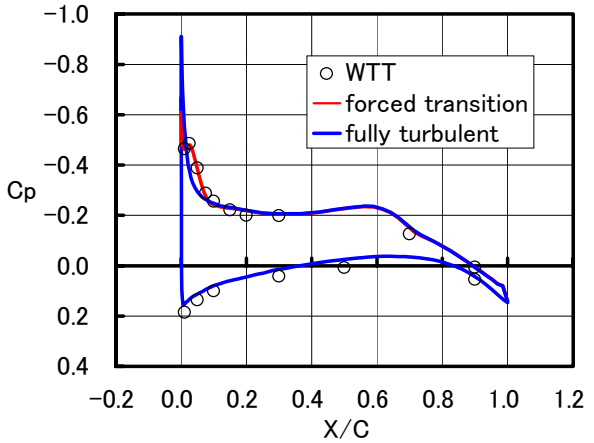

Fig.16 Comparison of pressure distributions at 50% span, M=0.95, α =2 °

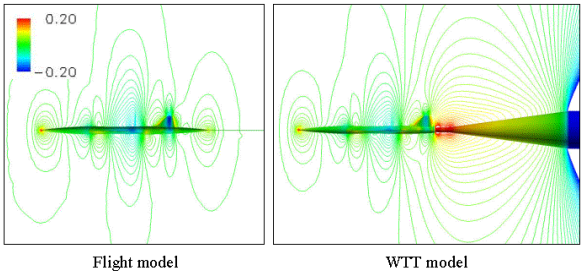

Fig.17 Comparison of pressure contours
at M=0.95, α =0 °

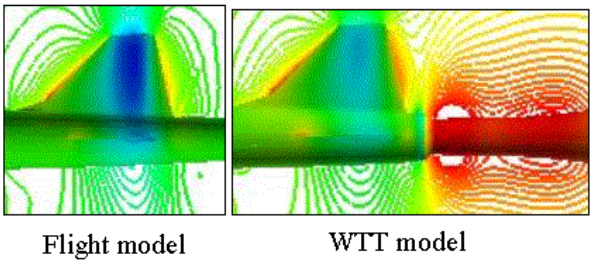

Fig.18 Comparison of pressure contours
at M=0.95, α =0 ° (enlarged view around tail)

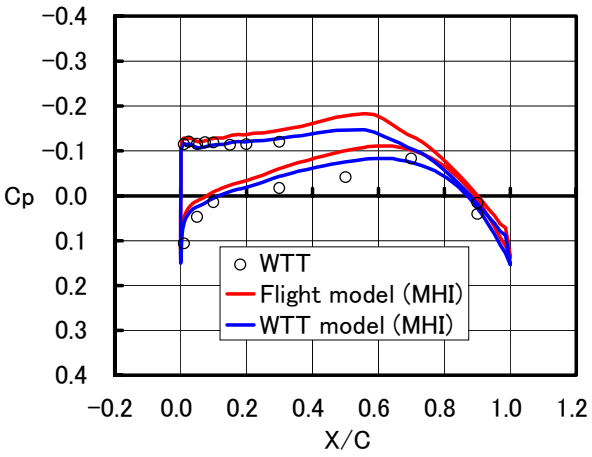

Fig.19 Comparison of pressure distributions at 50% span,
M=0.95, α =0 °

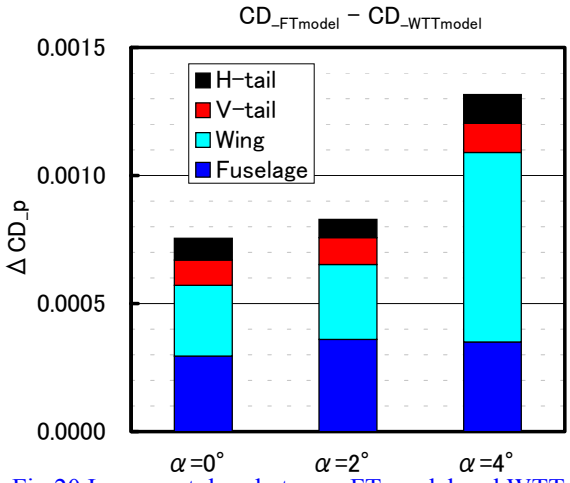

Fig.20 Increment drag between FT model and WTT model

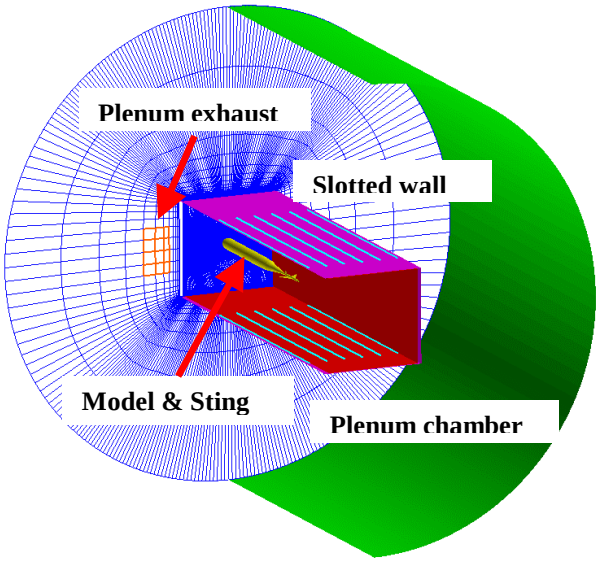

Fig.21 Computational grid of JAXA transonic WT

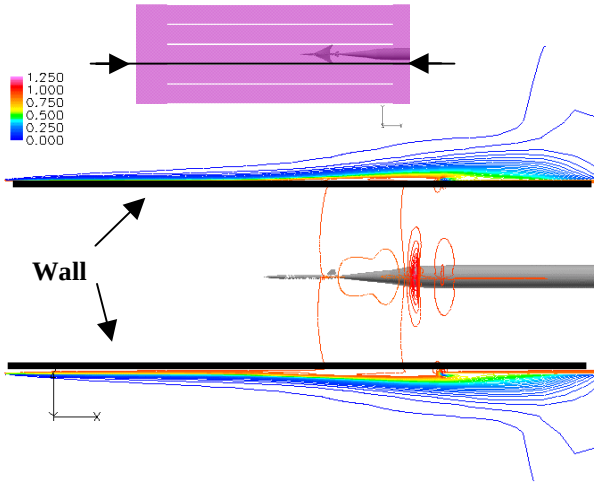

Fig.22 Mach number distribution at slot located plane,
M=0.95, α =0 ° (side view)

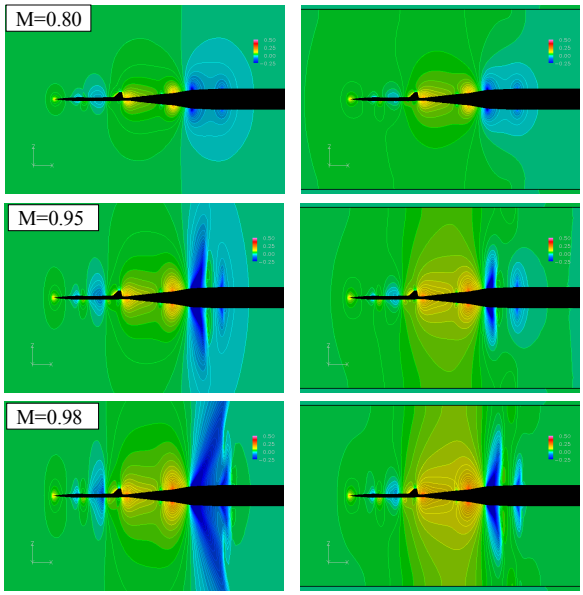

Fig.23 Comparison of pressure contours at α=0 °
[Left: Free-air (with sting) Right: Slotted wall]

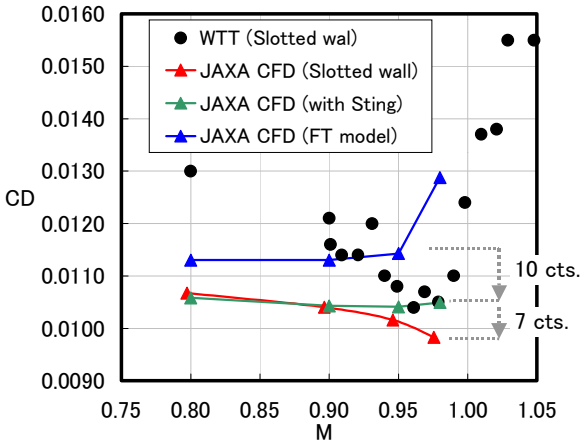

Fig.24 Drag divergence characteristics at α=0 °